# Nickel based hardfacing alloys for high temperature applications

*Conventional nickel based hardfacing alloys deposited by arc welding usually have a nominally single phase microstructure and derive their hot strength primarily from solid solution strengthening. The present work is an attempt at designing improved alloys containing large volume fractions of ordered precipitates or intermetallic compounds. The alloy design has been carried out using a computer model capable of estimating microstructure and strength as a function of many variables. The results are tested experimentally against cast samples which simulate welding conditions during manual metal arc welding.* MST/1035

S. Atamert
H. K. D. H. Bhadeshia

© *1989 The Institute of Metals. Manuscript received 21 December 1988; in final form 3 April 1989.* *The authors are in the Department of Materials Science and Metallurgy, University of Cambridge.*

## Introduction

Conventional nickel based hardfacing alloys are typically single phase alloys used where the component does not operate at high temperatures for prolonged periods of time. The alloys are usually deposited by arc welding techniques and provide a tough surface, resistant to wear, oxidation, and corrosion, which may work harden during service. The alloys cannot maintain their strength at very high temperatures (e.g. 800 °C) because they rely mainly on solid solution strengthening.

There have been some attempts to strengthen the alloys by the addition of boron and carbon,[1] but the modified alloys are not as popular as cobalt based hardfacing alloys. Unlike the nickel based superalloys used in aircraft engines, the alloys used for hardfacing do not for some reason contain aluminium or titanium. It is well established that the addition of these elements leads to the formation of ordered $\gamma'(Ni_3(Al, Ti))$ precipitates in the face centred cubic (fcc) $\gamma$ matrix. Some nickel based superalloys also contain topologically closed packed (tcp) phases (e.g. $\sigma$, $\mu$, $\chi$, and Laves phases) depending on composition and heat treatment. These hard phases are generally avoided owing to their detrimental effects on mechanical properties such as toughness. However, in the context of hardfacing materials they may increase wear resistance through their high hardness.[1] The design of new alloys tends to be costly and time consuming because of the large number of variables that must be taken into account. The aim of this study is to investigate new alloys, which are hardened either by $\gamma'$ or tcp phases, on the basis of an alloy design model which is capable of accounting for the simultaneous effects of several alloy additions and to confirm the predicted microstructures using simulated weld deposits. Of course, much further work is required to ensure that consumables which are easy to use can be developed. There is also a possibility that alloys containing high volume fractions of $\gamma'$ may be susceptible to cracking on heat treatment (such that could arise during multirun welding) and all this requires further investigation.

## Computer model for alloy design

The procedure used here for alloy design is based on the work of Harada *et al.*,[2] Yamazaki,[3] and Yamagata *et al.*[4] and is shown in Fig. 1. This method is capable of estimating the volume fractions and compositions of $\gamma$ and $\gamma'$ as a function of alloy chemistry, together with the lattice mismatch between the phases. In addition, it can also predict whether the alloy concerned is susceptible to the precipitation of intermetallic compounds.

For a specified alloy composition, the calculation begins with a guessed value of the $\gamma'$ volume fraction. If a partitioning ratio $R_i$ is defined for element $i$ as the ratio of its mole fraction in $\gamma$ to that in $\gamma'$, then values of $R_i$ (*see* Table 1) can be used in combination with mass balance conditions to estimate the composition of $\gamma'$

$$x_i^T = x_i^{\gamma'} V_{\gamma'} + x_i^{\gamma}(1 - V_{\gamma'}) \quad . \quad . \quad . \quad . \quad . \quad . \quad . \quad . \quad . \quad . \quad (1)$$

and

$$x_i^{\gamma} = x_i^{\gamma'} R_i \quad . \quad . \quad . \quad . \quad . \quad . \quad . \quad . \quad . \quad . \quad . \quad . \quad . \quad (2)$$

therefore

$$x_i^{\gamma'} = x_i^T / \{V_{\gamma'} + (1 - V_{\gamma'}) R_i\} \quad . \quad . \quad . \quad . \quad . \quad . \quad . \quad . \quad . \quad (3)$$

where $x_i^T$ is the average concentration of the $i$th element, $R_i (= x_i^{\gamma}/x_i^{\gamma'})$ is the partitioning coefficient, and $V_{\gamma'}$ is the mole fraction of $\gamma'$ precipitates. However, this estimated composition relies on a guessed value of $\gamma'$, and must be corrected iteratively by comparison with the equilibrium composition of $\gamma'$ as given by the 'phase diagram'. A $\gamma'$ surface has been defined as a surface in a multicomponent phase diagram on which the equilibrium compositions are connected to a corresponding $\gamma$ surface by tie lines (Fig. 2).[4] Using data[2] from 100 nickel based superalloys it is found that the aluminium concentration (at.-%) in $\gamma'$ as a function of other alloying elements, excluding nickel, in $\gamma'$ is given by[2]

$$y_{Al}^{\gamma'} = 29{\cdot}203 - 1{\cdot}096 x_{Cr}^{\gamma'} - 1{\cdot}195 x_{W}^{\gamma'} - 1{\cdot}220 x_{Ti}^{\gamma'} - 1{\cdot}066 x_{Ta}^{\gamma'} - 1{\cdot}950 x_{Mo}^{\gamma'} - 1{\cdot}446 x_{Nb}^{\gamma'} \quad . \quad (4)$$

The mole fraction of aluminium in $\gamma'$ ($x_{Al}^{\gamma'}$) calculated using the partitioning coefficients is compared with that calculated using the surface equation $y_{Al}^{\gamma'}$. If $x_{Al}^{\gamma'} - y_{Al}^{\gamma'} < 0{\cdot}001$, then the correct $\gamma'$ volume fraction is assumed to have been attained. If the difference is greater than 0·001, the initial guess value is modified using the Newton–Raphson iteration method.[5] Figure 3 shows a comparison between observed values of volume fraction (using data in Table 2) and predicted values.

**Table 1 Partitioning ratios for alloying elements, when $\gamma$ and $\gamma'$ are in equilibrium**

| Element | Cr | Mo | Al | Ti | Co | W | Ta |
|---|---|---|---|---|---|---|---|
| $R_i$ | 7·37 | 3·99 | 0·24 | 0·19 | 2·65 | 1·76 | 0·20 |

$R_i$ values are determined by the composition of the $\gamma$ phase through regression analyses using data from approximately one hundred nickel based superalloys.[2]

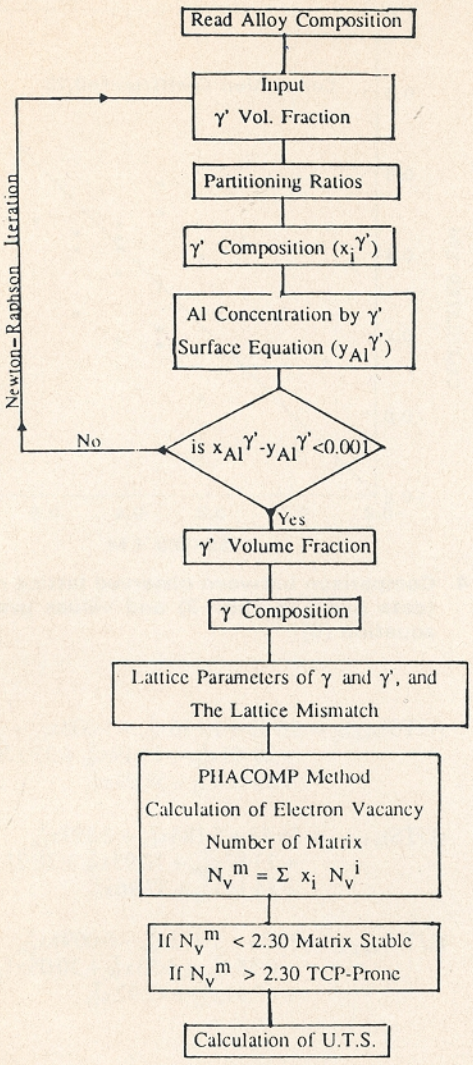


**1 Flow chart of computer program used in design of new nickel based hardfacing alloys**

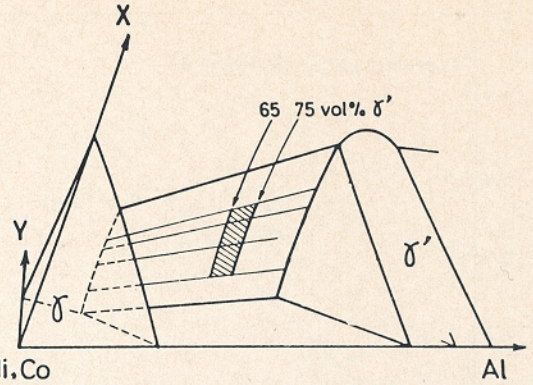


**2 Pseudoquaternary phase diagram showing γ and γ' surfaces; X and Y represent solid solution elements Cr, W, Mo, etc.[4]**

Since the lattice parameters of each phase depend on its chemical composition, multiple regression analysis was carried out for the alloys given in Table 3 to obtain values of per cent lattice mismatch (%LM)

$$(a_{\gamma'}-a_{\gamma}/a_{\gamma'})100 = 1{\cdot}216-0{\cdot}00202x_{Ni}^{T}+0{\cdot}003697x_{Cr}^{T}+0{\cdot}1090x_{Mo}^{T}+0{\cdot}07708x_{Al}^{T}-0{\cdot}04055x_{Ti}^{T}-0{\cdot}006479x_{Co}^{T}-0{\cdot}03787x_{W}^{T}-0{\cdot}003563x_{Ta}^{T} \quad . . . . . (5)$$

where $a_\gamma$ and $a_{\gamma'}$ are the lattice parameters of $\gamma$ between $\gamma'$ phases and $x_i^T$ represents the weight fraction of the $i$th element. A comparison between published experimental data and data estimated using equation (5) is shown in Fig. 4.

The phase computation method (PHACOMP) has also been applied (Fig. 1) to predict the presence or absence of tcp phases. This model suggests that tcp phases form after the critical value of the electron vacancy concentration $N_v^{crit}$ of the matrix has been exceeded. The value of $N_v^{crit}$ depends on the composition and temperature. It is taken to be 2·30, a value which is known to be a reasonable assumption.[8] For values greater than $N_v^{crit}$, the matrix is considered to be unstable and tcp phases may form.

**Table 2 Chemical composition and corresponding observed values of volume fraction of γ' precipitates $V_{\gamma'}$ for nickel based superalloys**

| Composition, wt-% | | | | | | | | | |
|---|---|---|---|---|---|---|---|---|---|
| Ni | Cr | Mo | Al | Ti | Co | W | Fe | $V_{\gamma'}$ | Ref. no. |
| 60·10 | 5·5 | 0·0 | 5·2 | 0·0 | 7·5 | 16·6 | 5·1 | 0·65 | 4 |
| 40·10 | 5·5 | 0·0 | 5·3 | 0·0 | 7·3 | 18·6 | 3·4 | 0·65 | |
| 68·0 | 6·6 | 0·0 | 5·2 | 0·0 | 0·0 | 12·8 | 7·7 | 0·65 | |
| 67·6 | 5·4 | 0·0 | 5·5 | 0·0 | 0·0 | 9·4 | 12·4 | 0·75 | |
| 69·25 | 9·0 | 1·0 | 5·75 | 1·2 | 0·0 | 10·5 | 3·3 | 0·69 | |
| 66·6 | 8·0 | 0·6 | 5·6 | 0·9 | 4·6 | 7·9 | 5·8 | 0·64 | |
| 66·5 | 8·5 | 0·0 | 5·5 | 2·2 | 5·5 | 9·5 | 2·8 | 0·68 | 6 |
| 68·1 | 6·7 | 0·0 | 4·7 | 0·0 | 0·0 | 7·7 | 12·8 | 0·74 | |
| 68·0 | 8·3 | 0·0 | 5·2 | 2·1 | 4·9 | 8·7 | 2·8 | 0·63 | |
| 61·3 | 5·7 | 0·0 | 4·4 | 0·0 | 7·6 | 16·2 | 4·8 | 0·55 | |
| 69·4 | 8·8 | 1·0 | 5·8 | 1·2 | 0·0 | 10·5 | 3·3 | 0·80 | |
| 54·5 | 15·0 | 0·0 | 2·6 | 4·5 | 13·4 | 10·0 | 0·0 | 0·511 | 2 |
| 58·3 | 12·1 | 0·0 | 3·2 | 5·7 | 11·9 | 8·8 | 0·0 | 0·65 | |
| 58·8 | 12·8 | 0·0 | 3·7 | 3·9 | 9·5 | 8·7 | 2·6 | 0·65 | |
| 62·3 | 5·8 | 0·0 | 4·0 | 3·1 | 8·5 | 13·3 | 3·0 | 0·65 | |
| 63·1 | 4·8 | 0·0 | 4·5 | 3·5 | 7·9 | 12·9 | 3·3 | 0·75 | |
| 58·7 | 9·7 | 0·0 | 4·3 | 0·6 | 8·9 | 13·2 | 3·8 | 0·50 | |
| 59·8 | 8·0 | 0·0 | 5·2 | 0·7 | 8·2 | 12·6 | 4·5 | 0·65 | |
| 59·4 | 8·2 | 0·0 | 4·8 | 0·0 | 8·2 | 12·7 | 4·9 | 0·65 | |
| 59·8 | 4·8 | 0·0 | 5·0 | 0·8 | 7·3 | 18·7 | 2·7 | 0·65 | |
| 63·7 | 8·0 | 6·0 | 6·0 | 0·7 | 10·0 | 0·0 | 4·3 | 0·732 | |
| 60·1 | 8·3 | 0·6 | 5·5 | 1·0 | 10·0 | 10·0 | 3·0 | 0·614 | |
| 62·8 | 6·1 | 2·0 | 5·4 | 1·0 | 7·5 | 5·8 | 9·0 | 0·745 | |

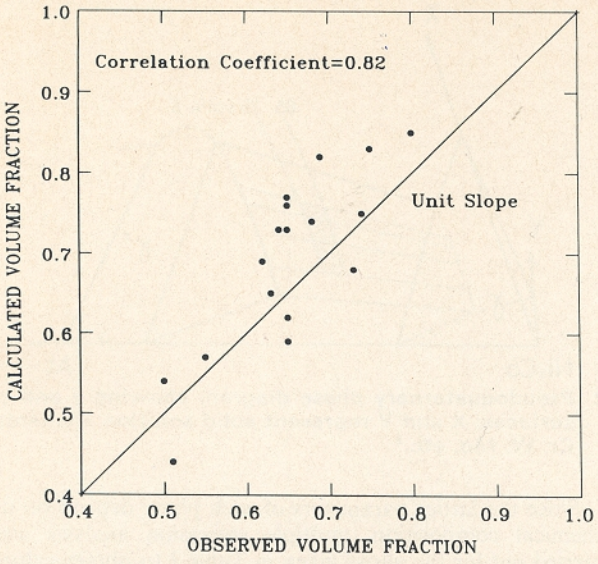


**3 Comparison between observed values of volume fraction of γ′ precipitates (data given in Table 2) and values predicted using equation (4)**

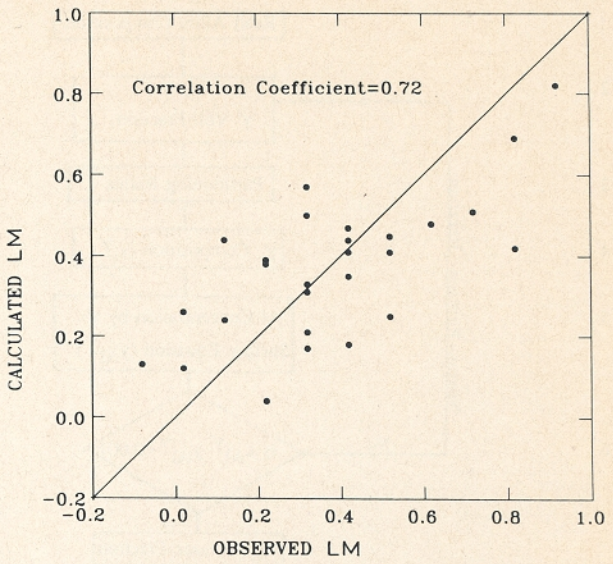


**4 Comparison between observed lattice mismatch LM (data given in Table 3) and values predicted using equation (5)**

Finally, the data from the alloy design model are used to estimate the ultimate tensile strength (UTS, MN m$^{-2}$) as a function of alloy composition (wt-%) at various temperatures using equations (6)–(10)

$$(\mathrm{UTS})_{20\,^\circ\mathrm{C}} = 461{\cdot}9 + 12{\cdot}91x^{\mathrm{T}}_{\mathrm{Cr}} + 2{\cdot}473x^{\mathrm{T}}_{\mathrm{Co}} + 15{\cdot}85x^{\mathrm{T}}_{\mathrm{Mo}} + 9{\cdot}621x^{\mathrm{T}}_{\mathrm{W}} + 26{\cdot}95x^{\mathrm{T}}_{\mathrm{Ta}} + 34{\cdot}44x^{\mathrm{T}}_{\mathrm{Al}} + 32{\cdot}51x^{\mathrm{T}}_{\mathrm{Ti}} \quad (6)$$

$$(\mathrm{UTS})_{650\,^\circ\mathrm{C}} = 148{\cdot}2 + 11{\cdot}39x^{\mathrm{T}}_{\mathrm{Cr}} + 4{\cdot}088x^{\mathrm{T}}_{\mathrm{Co}} + 14{\cdot}82x^{\mathrm{T}}_{\mathrm{Mo}} + 11{\cdot}80x^{\mathrm{T}}_{\mathrm{W}} + 29{\cdot}21x^{\mathrm{T}}_{\mathrm{Ta}} + 82{\cdot}19x^{\mathrm{T}}_{\mathrm{Al}} + 61{\cdot}05x^{\mathrm{T}}_{\mathrm{Ti}} \quad (7)$$

$$(\mathrm{UTS})_{760\,^\circ\mathrm{C}} = 96{\cdot}52 + 12{\cdot}16x^{\mathrm{T}}_{\mathrm{Cr}} + 1{\cdot}008x^{\mathrm{T}}_{\mathrm{Co}} + 20{\cdot}40x^{\mathrm{T}}_{\mathrm{Mo}} + 15{\cdot}19x^{\mathrm{T}}_{\mathrm{W}} + 33{\cdot}17x^{\mathrm{T}}_{\mathrm{Ta}} + 88{\cdot}68x^{\mathrm{T}}_{\mathrm{Al}} + 58{\cdot}92x^{\mathrm{T}}_{\mathrm{Ti}} \quad (8)$$

$$(\mathrm{UTS})_{871\,^\circ\mathrm{C}} = 56{\cdot}53 + 5{\cdot}184x^{\mathrm{T}}_{\mathrm{Cr}} + 2{\cdot}559x^{\mathrm{T}}_{\mathrm{Co}} + 23{\cdot}87x^{\mathrm{T}}_{\mathrm{Mo}} + 12{\cdot}93x^{\mathrm{T}}_{\mathrm{W}} + 28{\cdot}21x^{\mathrm{T}}_{\mathrm{Ta}} + 84{\cdot}14x^{\mathrm{T}}_{\mathrm{Al}} + 37{\cdot}96x^{\mathrm{T}}_{\mathrm{Ti}} \quad (9)$$

$$(\mathrm{UTS})_{982\,^\circ\mathrm{C}} = 37{\cdot}23 - 3{\cdot}992x^{\mathrm{T}}_{\mathrm{Cr}} - 0{\cdot}0091x^{\mathrm{T}}_{\mathrm{Co}} - 0{\cdot}55x^{\mathrm{T}}_{\mathrm{Mo}} + 6{\cdot}53x^{\mathrm{T}}_{\mathrm{W}} + 20{\cdot}05x^{\mathrm{T}}_{\mathrm{Ta}} + 67{\cdot}91x^{\mathrm{T}}_{\mathrm{Al}} + 42{\cdot}92x^{\mathrm{T}}_{\mathrm{Ti}} \quad (10)$$

**Table 3 Chemical composition and corresponding lattice mismatch (LM) for alloys used in multiple regression analysis**

| Per cent lattice mismatch (%LM) | Composition, wt-% | | | | | | | | |
|---|---|---|---|---|---|---|---|---|---|
| | Ni | Cr | Mo | Al | Ti | Co | W | Ta | Ref. no. |
| 0·32 | 60·10 | 5·5 | 0·0 | 5·2 | 0·0 | 7·5 | 16·6 | 5·1 | 4 |
| 0·17 | 40·10 | 5·5 | 0·0 | 5·3 | 0·0 | 7·3 | 18·6 | 3·4 | |
| 0·49 | 68·0 | 6·6 | 0·0 | 5·2 | 0·0 | 0·0 | 12·8 | 7·7 | |
| 0·28 | 66·40 | 9·2 | 0·0 | 5·3 | 0·0 | 0·0 | 8·7 | 10·4 | |
| 0·78 | 67·6 | 5·4 | 0·0 | 5·5 | 0·0 | 0·0 | 9·4 | 12·4 | |
| −0·04 | 69·25 | 9·0 | 1·0 | 5·75 | 1·2 | 0·0 | 10·5 | 3·3 | |
| 0·39 | 66·6 | 8·0 | 0·6 | 5·6 | 0·9 | 4·6 | 7·9 | 5·8 | |
| 0·28 | 62·5 | 10·0 | 0·0 | 5·0 | 1·5 | 5·0 | 4·0 | 12·0 | |
| 0·25 | 66·5 | 8·5 | 0·0 | 5·5 | 2·2 | 5·5 | 9·5 | 2·8 | |
| 0·35 | 68·1 | 6·7 | 0·0 | 4·7 | 0·0 | 0·0 | 7·7 | 12·8 | 7 |
| 0·16 | 68·0 | 8·3 | 0·0 | 5·2 | 2·1 | 4·9 | 8·7 | 2·8 | |
| 0·08 | 61·3 | 5·7 | 0·0 | 4·4 | 0·0 | 7·6 | 16·2 | 4·8 | |
| −0·56 | 69·4 | 8·8 | 1·0 | 5·8 | 1·2 | 0·0 | 10·5 | 3·3 | |
| −0·04 | 69·25 | 9·0 | 1·0 | 5·75 | 1·2 | 0·0 | 10·5 | 3·3 | |
| 0·393 | 87·20 | 0·0 | 0·0 | 12·8 | 0·0 | 0·0 | 0·0 | 0·0 | |
| 0·5635 | 87·30 | 0·0 | 0·0 | 12·7 | 0·0 | 0·0 | 0·0 | 0·0 | |
| 0·521 | 87·81 | 0·0 | 0·0 | 12·19 | 0·0 | 0·0 | 0·0 | 0·0 | |
| 0·449 | 87·70 | 0·0 | 0·0 | 12·30 | 0·0 | 0·0 | 0·0 | 0·0 | |
| 0·056 | 75·90 | 18·7 | 0·0 | 5·4 | 0·0 | 0·0 | 0·0 | 0·0 | |
| 0·244 | 84·30 | 5·2 | 0·0 | 10·50 | 0·0 | 0·0 | 0·0 | 0·0 | |
| 0·398 | 79·3 | 9·9 | 0·0 | 10·8 | 0·0 | 0·0 | 0·0 | 0·0 | |
| 0·918 | 77·80 | 15·0 | 0·0 | 2·4 | 4·5 | 0·2 | 0·0 | 0·0 | |
| 0·779 | 76·70 | 15·1 | 1·0 | 2·5 | 4·5 | 0·2 | 0·0 | 0·0 | |
| 0·417 | 75·70 | 15·1 | 3·0 | 2·5 | 4·5 | 0·2 | 0·0 | 0·0 | |
| 0·724 | 73·80 | 21·9 | 0·0 | 1·90 | 2·4 | 0·0 | 0·0 | 0·0 | |
| 0·363 | 73·30 | 21·7 | 0·0 | 3·70 | 1·30 | 0·0 | 0·0 | 0·0 | |
| 0·028 | 73·00 | 20·6 | 0·0 | 6·3 | 0·0 | 0·0 | 0·0 | 0·0 | |
| 0·306 | 52·0 | 18·0 | 4·2 | 3·0 | 3·0 | 19·0 | 0·0 | 0·0 | |
| 0·640 | 71·0 | 21·0 | 0·0 | 2·8 | 2·8 | 0·5 | 0·0 | 0·0 | |

% LM = $(a_{\gamma'} - a_{\gamma}/a_{\gamma'})$ 100.

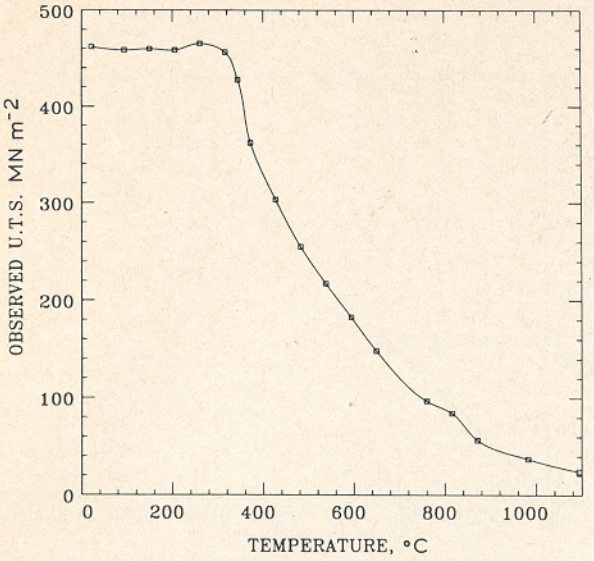


**5 Strength of pure nickel as function of temperature (data from Ref. 10)**

These equations were derived using multiple regression analysis of the data given in Table 4. The strengthening resulting from pure nickel was subtracted for each composition and used as a regression constant. Using this method, the contributions of the individual alloying elements to the strength of nickel based hardfacing alloys could be evaluated. The strength of pure nickel as a function of temperature is given in Table 5 and shown in Fig. 5. Figures 6*a*–6*e* show comparisons between observed values of UTS and values predicted using equations (6)–(10) at various temperatures. Correlation coefficients were found to be 0·84, 0·84, 0·83, 0·86, and 0·85 at 21, 650, 760, 871, and 982°C, respectively, showing the good agreement between observed and calculated values of UTS.

## Experimental alloys

Hastelloy type Ni–Cr–Mo hardfacing alloys with the nominal composition Ni–15Cr–16Mo (wt-%) are used currently for high temperature applications (e.g. hot shear blades, valve seats) where, in addition to the high temperature strength, oxidation and corrosion resistance are also important. These alloys are nominally single phase and include other alloying additions such as tungsten and iron. The composition of Hastelloy C276 which was deposited by the manual metal arc welding process is given in Table 6. The weld was deposited in three layers so that the top layer could be examined in an essentially undiluted condition. Electrodes 4 mm in diameter were used, the welding conditions being 160 A, 23 V AC, with a welding speed of about 0·004 m $s^{-1}$ and an interpass temperature of about 350°C.

In addition to this alloy deposited by arc welding, several aluminium and titanium containing samples were prepared as experimental casts (~ 65 g) made from high purity elements in an argon arc furnace with a water cooled copper mould. This casting method is known to simulate well the conditions arising during the solidification of manual metal arc hardfacing deposits.[11] The chemical compositions of the alloys studied are given in Table 6. A number of rods 3 mm in diameter were machined from the weld deposit, parallel to the welding direction. For heat treatment experiments, disc specimens of 3 mm diameter were cut from the casts and sealed in a quartz tube, after

**Table 4 Chemical composition and corresponding values of ultimate tensile strength (UTS) for cast nickel based superalloys used in multiple regression analysis[9]**

| UTS, MN $m^{-2}$ | | | | | Composition, wt-% | | | | | | | | |
|---|---|---|---|---|---|---|---|---|---|---|---|---|---|
| 20°C | 650°C | 760°C | 871°C | 982°C | Ni | Cr | Mo | Co | W | Ta | Al | Ti | Fe |
| 710 | 660 | ... | ... | ... | 63·0 | 15·5 | 0·0 | 5·3 | 0·0 | 0·0 | 3·0 | 2·0 | 10·0 |
| 500 | ... | ... | ... | ... | 73·0 | 20·0 | 0·0 | 0·0 | 0·0 | 0·0 | 0·2 | 0·4 | 5·0 |
| 730 | ... | ... | ... | ... | 71·0 | 20·0 | 0·0 | 0·0 | 0·0 | 0·0 | 1·3 | 2·4 | 5·0 |
| 700 | 560 | 490 | 260 | ... | 53·0 | 20·0 | 17·5 | 0·0 | 0·0 | 0·0 | 1·3 | 2·4 | 5·0 |
| 1040 | 1080 | 1195 | 1215 | 595 | 74·0 | 0·0 | 0·0 | 18·0 | 0·0 | 0·0 | 8·0 | 0·0 | 0·0 |
| 975 | 1015 | 950 | 793 | 550 | 64·0 | 8·0 | 10·0 | 6·0 | 0·0 | 4·0 | 6·0 | 1·0 | 0·0 |
| 1185 | ... | 1295 | 1020 | ... | 66·0 | 8·0 | 4·6 | 0·6 | 7·9 | 5·8 | 5·6 | 0·9 | 0·0 |
| 1015 | 1110 | 1070 | 885 | 565 | 60·0 | 10·0 | 15·0 | 3·0 | 0·0 | 0·0 | 5·5 | 4·7 | 0·0 |
| 835 | 895 | 915 | 750 | 525 | 67·0 | 9·5 | 10·0 | 2·5 | 0·0 | 0·0 | 5·5 | 4·6 | 0·0 |
| 1035 | 1085 | 965 | 770 | 455 | 61·0 | 16·0 | 8·5 | 1·7 | 2·6 | 1·7 | 3·4 | 3·4 | 0·0 |
| 1170 | ... | 1130 | 840 | ... | 61·0 | 12·4 | 9·0 | 1·9 | 3·8 | 3·9 | 3·1 | 4·5 | 0·0 |
| 1050 | 985 | 915 | 640 | 325 | 48·0 | 22·5 | 19·0 | 0·0 | 2·0 | 1·4 | 1·9 | 3·7 | 0·0 |
| 1170 | 1090 | 990 | 840 | ... | 61·0 | 12·4 | 9·0 | 1·9 | 3·8 | 3·9 | 3·1 | 4·5 | 0·0 |
| 730 | 835 | 910 | 885 | 545 | 71·0 | 5·7 | 0·0 | 2·0 | 11·0 | 3·0 | 6·3 | 0·0 | 0·0 |
| 930 | 950 | 930 | 840 | 550 | 60·0 | 9·0 | 10·0 | 0·0 | 12·0 | 0·0 | 5·0 | 2·0 | 0·0 |
| 1000 | 1020 | 1080 | 915 | 655 | 60·0 | 9·0 | 10·0 | 0·0 | 12·0 | 0·0 | 5·0 | 2·0 | 0·0 |
| 965 | 1035 | 1035 | 860 | 550 | 60·0 | 9·0 | 10·0 | 2·5 | 10·0 | 1·5 | 5·5 | 1·5 | 0·0 |
| 1035 | 1070 | 1035 | 825 | 550 | 61·0 | 9·0 | 10·0 | 0·0 | 10·0 | 2·5 | 5·5 | 1·5 | 0·0 |
| 1000 | 1000 | 895 | 655 | 380 | 74·0 | 12·0 | 0·0 | 4·5 | 0·0 | 0·0 | 5·9 | 0·6 | 0·0 |
| 1070 | 1070 | 1070 | 860 | 550 | 59·0 | 8·5 | 10·0 | 2·0 | 8·0 | 3·8 | 4·8 | 2·5 | 0·0 |
| 1105 | 1070 | 1070 | 860 | 565 | 63·0 | 9·0 | 10·0 | 2·5 | 10·0 | 1·5 | 5·5 | 1·5 | 0·0 |
| 1035 | 1070 | 1035 | 825 | 540 | 59·0 | 9·0 | 10·0 | 0·0 | 12·5 | 0·0 | 5·0 | 2·0 | 0·0 |
| 1085 | ... | 1135 | 950 | ... | 60·0 | 8·3 | 10·0 | 0·7 | 10·0 | 3·0 | 5·5 | 1·0 | 0·0 |
| 965 | 1050 | 1035 | 825 | 550 | 60·0 | 8·2 | 10·0 | 0·0 | 10·0 | 3·0 | 5·5 | 1·0 | 0·0 |
| 1140 | 1140 | 1130 | 995 | 685 | 63·0 | 10·0 | 5·0 | 0·0 | 4·0 | 12·0 | 5·0 | 1·5 | 0·0 |
| 1020 | 1050 | 940 | ... | ... | 58·0 | 14·6 | 15·0 | 4·2 | 0·0 | 0·0 | 4·3 | 3·3 | 0·0 |
| 1030 | 1030 | 995 | 705 | ... | 60·0 | 14·0 | 9·5 | 4·0 | 4·0 | 0·0 | 3·0 | 5·0 | 0·0 |
| 1020 | 910 | 875 | ... | ... | 51·0 | 15·0 | 22·0 | 4·5 | 0·0 | 0·0 | 4·4 | 2·4 | 0·0 |
| 1060 | 1100 | 1090 | 840 | ... | 58·0 | 11·0 | 14·5 | 6·5 | 1·5 | 0·0 | 5·4 | 2·5 | 0·0 |
| 1050 | 1140 | 1095 | 870 | 595 | 61·0 | 6·1 | 7·5 | 2·0 | 5·8 | 9·0 | 5·4 | 1·0 | 0·0 |
| 930 | 885 | 855 | 650 | 130 | 52·0 | 18·0 | 19·0 | 4·2 | 0·0 | 0·0 | 3·0 | 3·0 | 0·0 |
| 945 | 950 | 945 | 710 | ... | 64·0 | 16·0 | 5·0 | 1·5 | 6·0 | 0·0 | 4·5 | 2·0 | 0·0 |
| 1075 | 1110 | 1055 | 730 | 415 | 55·0 | 18·0 | 15·0 | 3·0 | 15·0 | 0·0 | 2·5 | 5·0 | 0·0 |
| 895 | 830 | 830 | 775 | 485 | 72·0 | 0·0 | 0·0 | 0·0 | 20·0 | 0·0 | 6·5 | 0·0 | 0·0 |
| 1040 | 1080 | 1195 | 1215 | 595 | 74·0 | 0·0 | 0·0 | 18·0 | 0·0 | 0·0 | 8·0 | 0·0 | 0·0 |

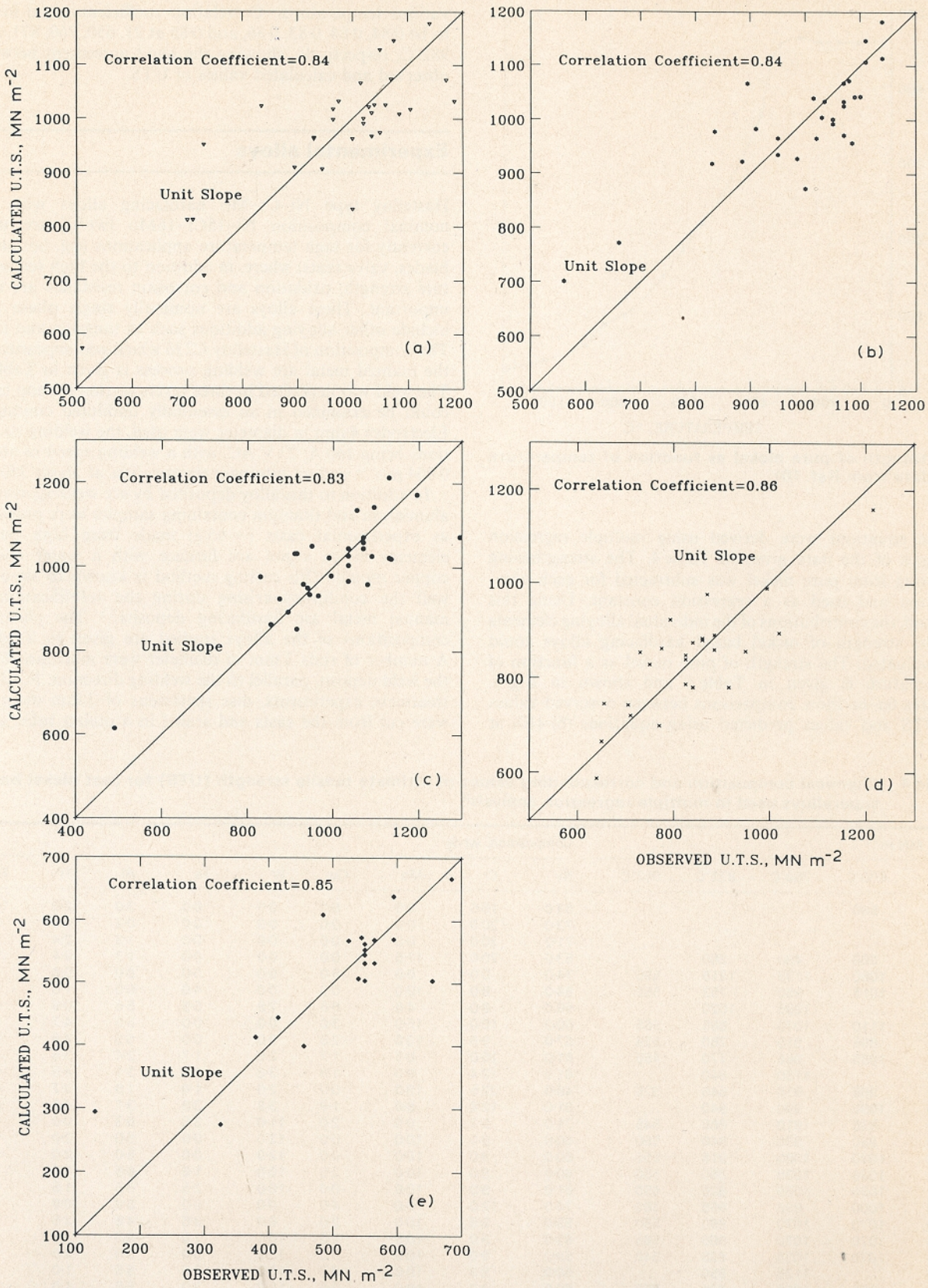


*a* room temperature; *b* 650°C; *c* 760°C; *d* 871°C; *e* 982°C

**6 Comparison between observed values of UTS (*see* Table 4) and values calculated using equations (6)–(10) at various temperatures**

flushing three times with argon, pumping down to a pressure of $10^{-6}$ torr and backfilling with a partial pressure of argon. The alloy compositions were selected on the basis of calculations using the computer model and the results are given in Table 7, including values of ultimate tensile strength as a function of temperature. The electron vacancy concentration of the matrix phase $N_v^m$ is also calculated and compared with the critical electron vacancy

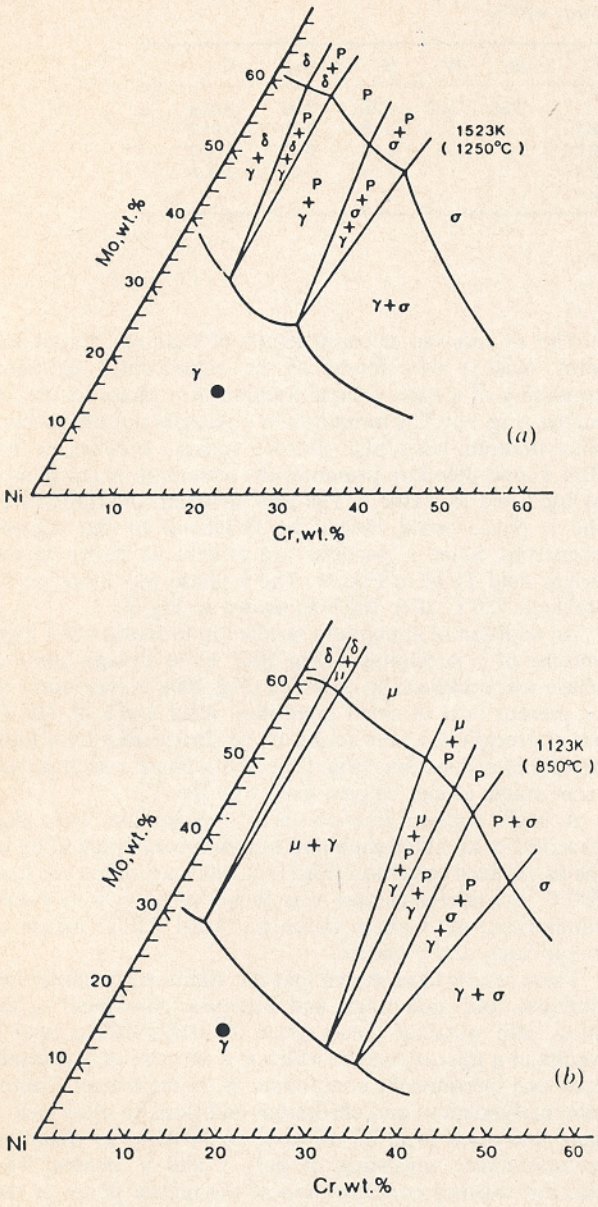


*a* 1250°C; *b* 850°C
● location of alloy C 276

**7 Isothermal sections of Ni–Cr–Mo system[12]**

**Table 5 Ultimate tensile strength (UTS) of annealed pure nickel as function of temperature[10]**

| Temperature, °C | UTS, MN m$^{-2}$ |
|---|---|
| 21 | 461 |
| 93 | 458 |
| 149 | 459 |
| 204 | 458 |
| 260 | 465 |
| 315 | 456 |
| 343 | 427 |
| 371 | 361 |
| 426 | 303 |
| 482 | 255 |
| 538 | 217 |
| 593 | 182 |
| 649 | 148 |
| 760 | 96 |
| 815 | 84 |
| 871 | 56 |
| 982 | 37 |
| 1093 | 24 |

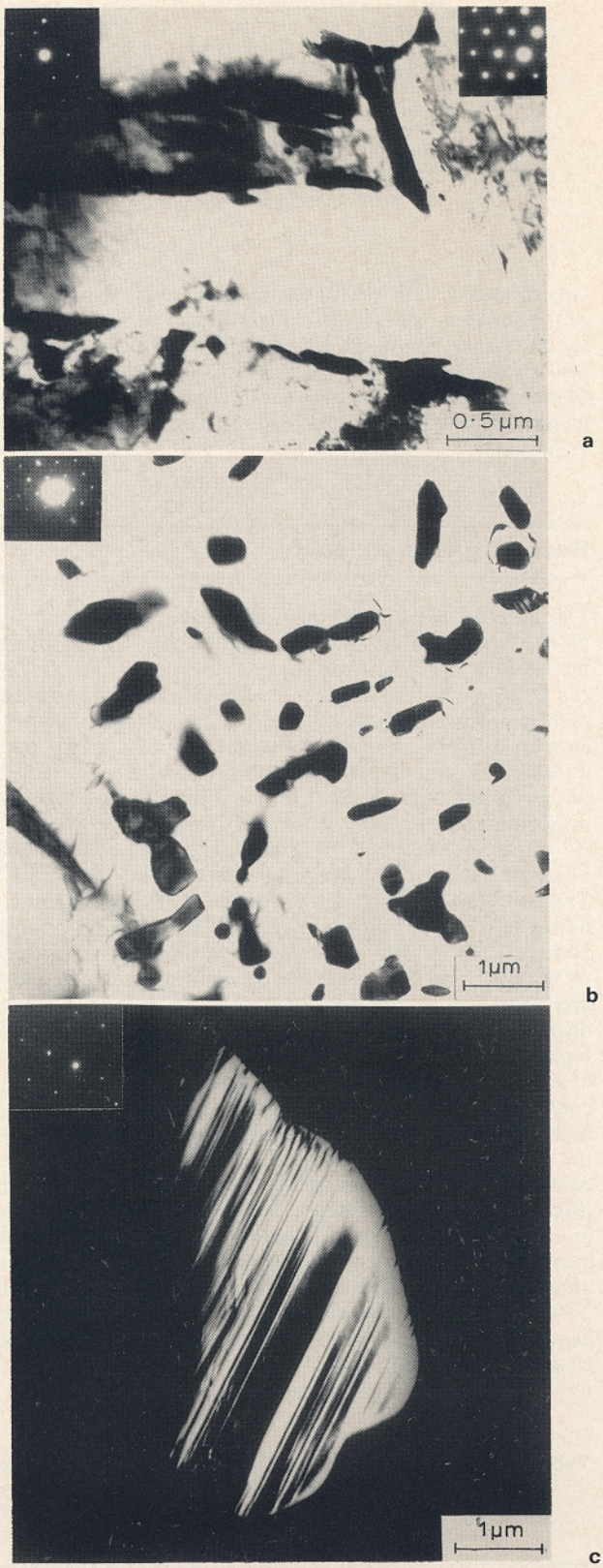


*a* bright field TEM showing fcc γ grain and P phase; selected area diffraction pattern (SADP) from P phase is shown in left hand inset (zone axis is $\langle 320 \rangle_P$) and SADP from matrix phase is shown in right hand inset (zone axis is $\langle 111 \rangle_{fcc}$); *b* bright field TEM after 20 d at 850°C showing two phase equilibrium, fcc matrix, and μ phase, indicating that P phase is not stable at this temperature; *c* dark field TEM of μ phase using (132) reflection showing extensive faults (zone axis of inset SADP is ⟨134⟩)

**8 Alloy C 276 after solidification and heat treatment**

**Table 6 Chemical composition of alloys studied, wt-%**

| Alloy | Ni | Cr | Mo | Al | Ti | Fe | W | Si | Mn | C |
|---|---|---|---|---|---|---|---|---|---|---|
| Hastelloy, C 276 | 62·6 | 14·94 | 15·48 | ... | ... | 2·25 | 3·78 | 0·26 | 0·58 | 0·068 |
| Cast 1 | 57·8 | 15·2 | 16·9 | 0·3 | 8·1 | ... | ... | 0·18 | 0·20 | 0·012 |
| Cast 2 | 63·1 | 15·4 | 15·7 | 5·2 | 0·02 | ... | ... | 0·13 | 0·20 | 0·008 |
| Cast 3 | 62·0 | 15·4 | 16·0 | 3·3 | 2·4 | ... | ... | 0·14 | 0·20 | 0·004 |
| Cast 4* | 74·0 | 10·0 | 10·0 | 3·3 | 2·4 | ... | ... | ... | ... | ... |

* Nominal composition.

concentration $N_v^{crit} = 2{\cdot}30$. The ratio $N_v^m/N_v^{crit}$ is a measure of the stability of the matrix phase. It can be seen that $N_v^m$ for all the cast alloys (except cast 4) studied is greater than 2·30 indicating that tcp phases are likely to form. The titanium containing alloys were found to be the most metastable as a result of the high electron vacancy number of titanium.

## Results and discussion

The location of alloy C276 in isothermal sections of the Ni–Cr–Mo system at 1250°C and 850°C (Ref. 12), ignoring the effect of other alloying elements, is shown in Fig. 7. It can be seen that the alloy is in the single phase fcc region at each temperature. However, transmission electron microscopy revealed that the alloy is a mixture of fcc matrix and intermetallic compound P phase, preferentially nucleated on $\gamma/\gamma$ grain boundaries (Fig. 8*a*). The P phase has an orthorhombic crystal structure with $a = 0{\cdot}907$ nm, $b = 1{\cdot}698$ nm, and $c = 0{\cdot}475$ nm.[8] This phase has been observed extensively in Hastelloy nickel based alloys.[12–14] The composition range (at.-%) of the P phase was determined to be 9·1–18·4%Cr, 31·2–34·5%Ni, and 50·4–58·2%Mo with a nominal chemical composition $CrNi_2Mo_2$ (Ref. 12). It has been demonstrated that alloy additions such as iron and tungsten in Hastelloy C276 can displace the $\gamma$ solvus line so that the alloy can be in $P+\gamma$ region as the alloy solidifies from 1250 to 850°C. The $P+\gamma$ field at 850°C is displaced to a region of higher chromium content as the $\mu+\gamma$ field appears at lower chromium and higher molybdenum concentrations. This is consistent with the experimental results which showed that the alloy contains $\mu$ phase in the fcc matrix at 850°C after 20 d (Fig. 8*b*). The $\mu$ phase has a hexagonal crystal structure ($a = 0{\cdot}476$ nm and $c = 2{\cdot}572$ nm) having a rhombohedral symmetry[12] with a high fault density (Fig. 8*c*). The appearance of the $\mu$ phase is not expected on the basis of a value of 2·30 for the critical electron vacancy number, but it is assumed that the $\mu$ phase arises because the alloy is fairly close to the limiting value of 2·3.

**Table 7 Calculated volume fraction of $\gamma'$ precipitates $V\gamma'$, ultimate tensile strength (UTS) as function of temperature, and $N_v^m/N_v^{crit}$ ratio of experimental alloys**

| | | UTS, MN m$^{-2}$ | | | | | |
|---|---|---|---|---|---|---|---|
| Alloy | $V\gamma'$ | 20°C | 650°C | 760°C | 871°C | 982°C | $N_v^m/N_v^{crit}$* |
| C276 | ... | 936 | 593 | 650 | 552 | ... | 0·89 |
| Cast 1 | 0·5 | 1199 | 1091 | 1124 | 871 | 335 | 1·22 |
| Cast 2 | 0·43 | 1106 | 978 | 1024 | 887 | 294 | 1·13 |
| Cast 3 | 0·55 | 1089 | 984 | 1066 | 949 | 321 | 1·25 |
| Cast 4 | 0·48 | 951 | 850 | 878 | 736 | 336 | 0·83 |

* $N_v^{crit} = 2{\cdot}30$.

The as received microstructure of titanium containing alloy (cast 1) was found to be significantly different, consisting of a high volume fraction of $\sigma$ phase in the fcc matrix (Fig. 9*a*). The formation of $\sigma$ phase is not unexpected since titanium has a high electron vacancy number, i.e. 6·6 (Ref. 8) and therefore promotes the formation of tcp phases as indicated in Table 7. The fine 'lamellar' distribution of the $\sigma$ phase could indeed be beneficial to the deposit properties. Some $\gamma'$ particles are evident as shown in the bright field TEM in Fig. 9*b*. The $\sigma$ phase was found to be stable at 750°C after 100 h as shown in Fig. 9*c*.

An addition of aluminium resulted in formation of a high volume of $\gamma'$ precipitates (Fig. 10*a*). Even though some $\sigma$ phase was occasionally observed (Fig. 10*b*), it was found to be present only in small quantities. After 100 h at 750°C, the $\gamma'$ precipitates were found to be surrounded by a high density of dislocations (Fig. 10*c*). The $\sigma$ phase was observed to be stable as can be seen from Fig. 10*c*.

A high volume fraction of $\gamma'$ precipitates was also observed in an aluminium and titanium containing alloy in the as received condition (Fig. 11*a*). After aging for 100 h at 750°C, the microstructure was found to be in four phase equilibrium, as $\sigma$ phase (large particles), $Ni_3Ti$ plates, $\gamma'$ precipitates, and $\gamma$ matrix.

These results have shown that the addition of aluminium, titanium, and aluminium and titanium (combined) to an alloy with nominal composition Ni–16Cr–16Mo (wt-%) results in a microstructure which is a mixture of $\gamma'$ precipitates and intermetallic compounds in an fcc matrix. Therefore, molybdenum and chromium additions to alloy cast 3 were decreased from 15–16 wt-% to 10 wt-% to obtain a microstructure consisting of only $\gamma$ and $\gamma'$ phases. The electron vacancy concentration of the matrix phase of the new alloy (cast 4) was found to be $\sim 1{\cdot}8$ which is much less than the value of $N_v^{crit}$ suggesting that intermetallic compounds are not likely to form. Results of TEM analysis were found to be consistent with the above discussion, showing that the alloy contains very fine $\gamma'$ precipitates with volume fraction $\sim 0{\cdot}6$ in the $\gamma$ matrix (Fig. 12). Although this result is very encouraging, the high temperature microstructural stability of this alloy has yet to be determined.

## Conclusions

A computer program which is capable of accounting for the simultaneous effects of several alloy additions has been used to design a number of nickel based alloys which have microstructures that should have better hardfacing properties when compared with conventional single phase alloys. The main purpose was to provide a precipitation strengthening via $\gamma'$ by the addition of aluminium and titanium. The program used is capable of calculating the volume fraction and composition of $\gamma'$ precipitates, the electron vacancy concentration of the matrix phase (which gives an indication of whether tcp phases will be stable), and various other characteristics including strength.

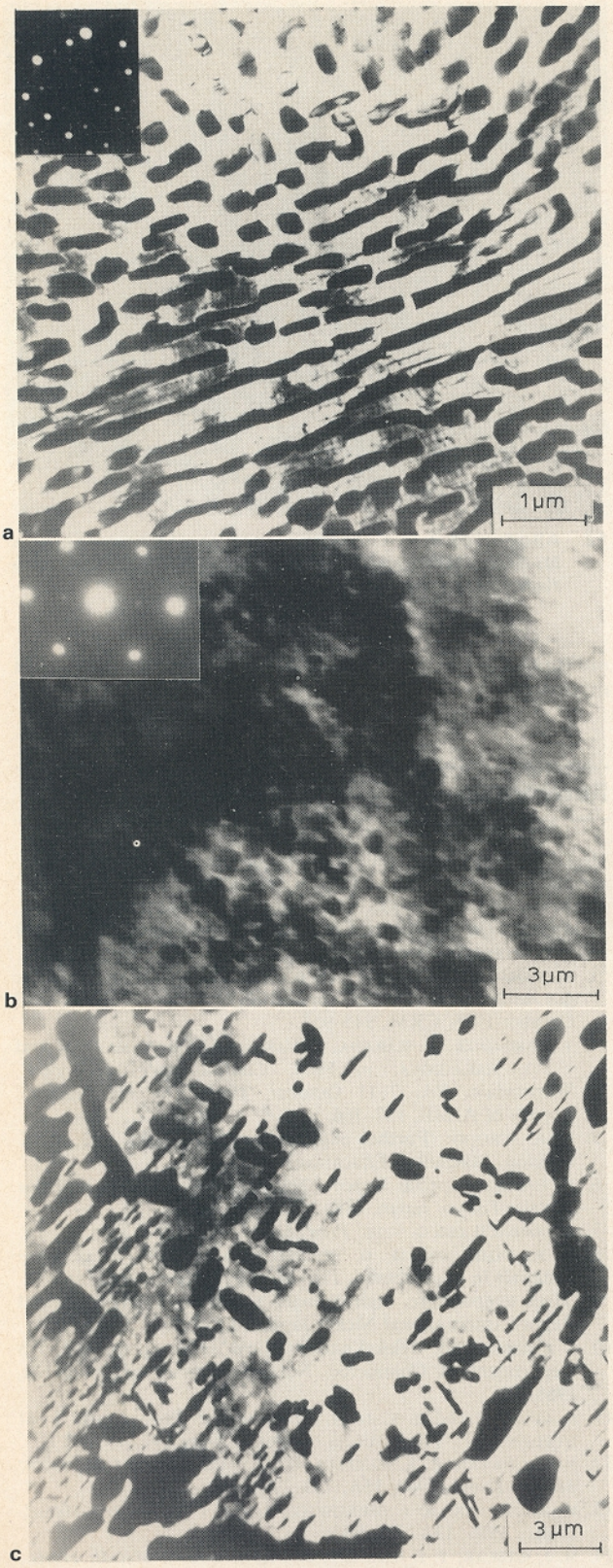


*a* high volume fraction of $\sigma$ phase; SADP from $\sigma$ phase is inset (zone axis is $\langle 111 \rangle_\sigma$); *b* $\gamma'$ precipitates; SADP from $\gamma/\gamma'$ region is inset (zone axis is $\langle 011 \rangle_{fcc}$); *c* after 100 h at 750°C, showing that $\sigma$ phase is stable and in equilibrium with $\gamma$ and $\gamma'$ phases

**9 Alloy cast 1, Ni–15·2Cr–16·9Mo–0·3Al–8·1Ti (wt-%), after solidification and heat treatment (bright field TEM)**

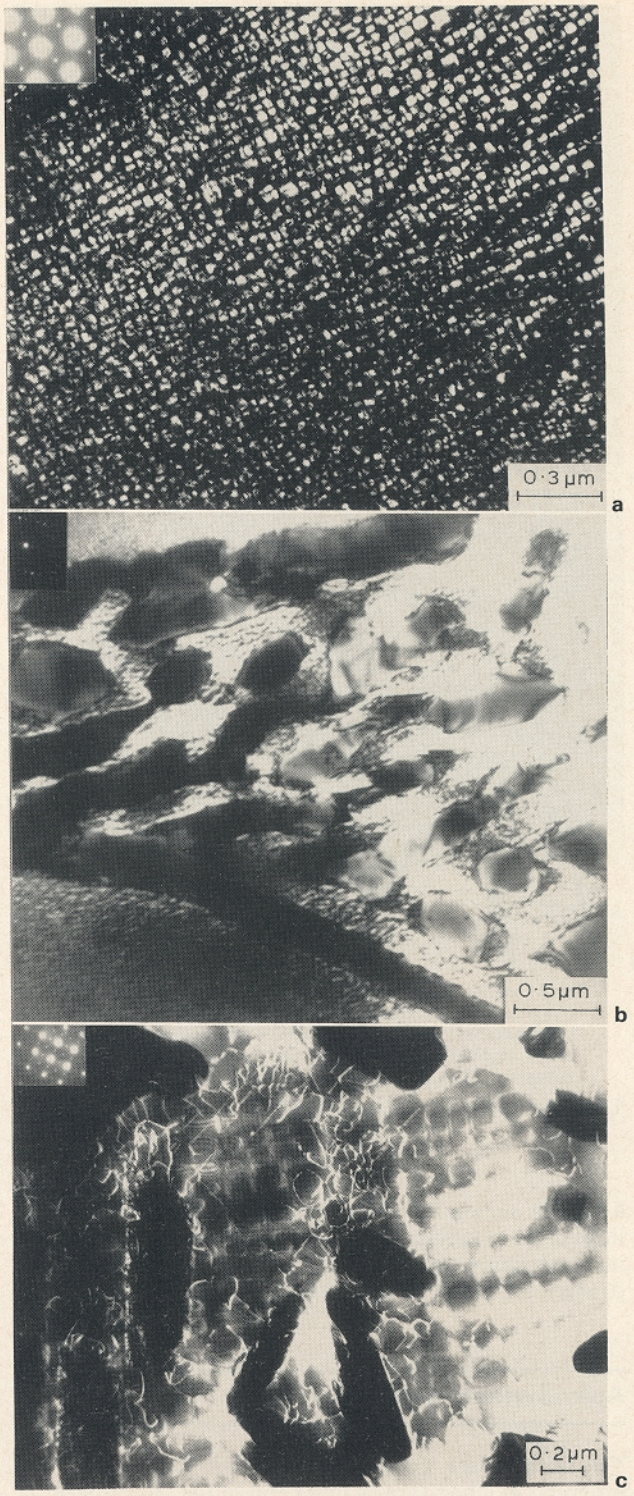


*a* dark field TEM obtained using $(110)_{\gamma'}$ reflection showing high volume fraction of $\gamma'$ precipitates ($\sim$ 0·6); zone axis is $\langle 011 \rangle_{\gamma'}$; *b* bright field TEM showing $\sigma$ phases (zone axis of inset SADP is $\langle 201 \rangle_\sigma$); *c* dark field TEM obtained using $(110)_{\gamma'}$ superlattice reflection showing high density of dislocations and some $\sigma$ phase (black particles)

**10 Alloy cast 2, Ni–15·4Cr–15·7Mo–5·2Al–0·02Ti (wt-%)**

The addition of aluminium, titanium, and aluminium and titanium in combination to an alloy with nominal composition Ni–16Cr–16Mo (wt-%) giving $\sim$ 0·6 volume fraction of $\gamma'$ precipitates was studied experimentally using a casting method as a simulation of manual metal arc deposits. These additions resulted in the formation of a high volume fraction of intermetallic compounds the morphology, volume fraction, and range of stability of which were found to vary significantly with composition. The actual effects of these intermetallic compounds on alloy mechanical properties is

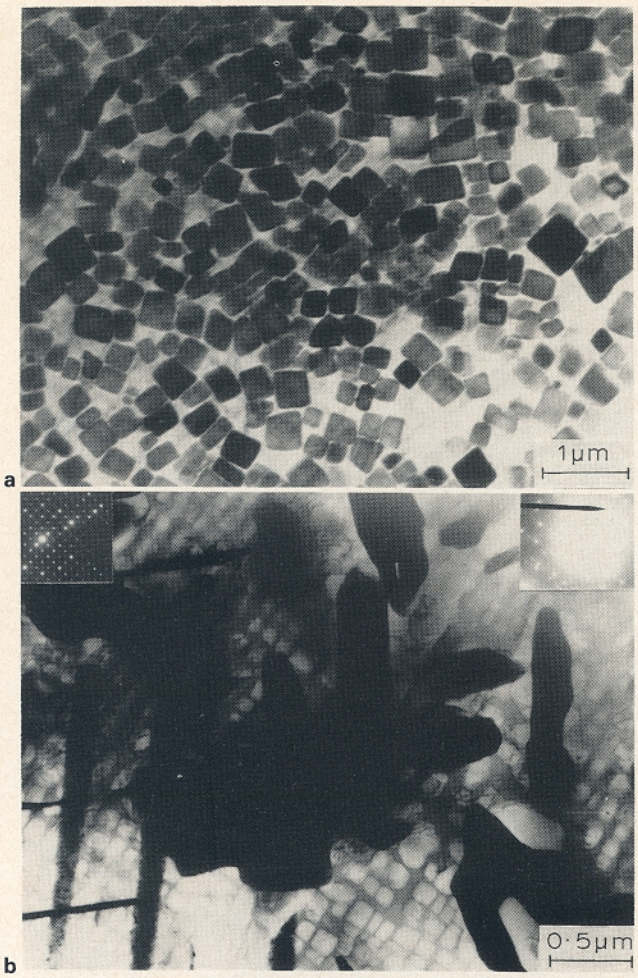


*a* as received microstructure consisting of $\gamma'$ precipitates; *b* after 100 h at 750°C showing four phase equilibrium: $\sigma$ phase (large black particles), left hand inset SADP with zone axis $\langle 110 \rangle_{\sigma}$; $Ni_3Ti$ plates, right hand inset SADP with zone axis $\langle 100 \rangle_{Ni_3Ti}$ (arrow indicates $(231)_{Ni_3Ti}$ spot); $\gamma'$ precipitates; and $\gamma$ matrix

**11 Alloy cast 3, Ni–15·4Cr–16·0Mo–3·3Al–2·4Ti(wt-%)**

a suitable subject for future research. In general, the predictions of the computer model are found to be consistent with microstructural observations, and the estimates of hot strength are found to be encouraging.

## Acknowledgments

The authors are grateful to Professor D. Hull for the provision of laboratory facilities and to the Government of Turkey for financial support. The alloys used were kindly provided by ESAB AB (manual metal arc welds). The authors are grateful to Dr L.-E. Svensson and Mr B. Ulander for arranging the provision of alloys and for their cooperation throughout the course of this work. The authors are especially grateful to Dr H. Harada for helpful discussions.

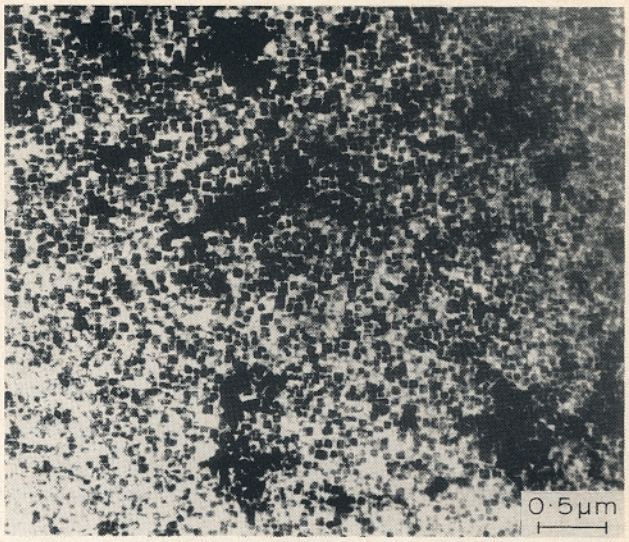


**12 Alloy cast 4 with nominal composition Ni–10Cr–10Mo–3·3Al–2·4Ti (wt-%) showing very fine $\gamma'$ precipitates (bright field TEM)**

## References

1. E. F. NIPPES (ed.): Metals Handbook, Vol. 6, 'Welding, brazing, and soldering', 9 edn, 771–803; 1983, Metals Park, OH, ASM.
2. H. HARADA, M. YAMAZAKI, K. KOIZUMI, N. SAKUMA, N. FURUYA, and H. KAMIYA: in Proc. Conf. on 'High temperature alloys for gas turbines', Liège, Belgium, 4–6 Oct. 1982, CRM, 721–735.
3. M. YAMAZAKI: in Proc. Conf. on 'High temperature alloys for gas turbines and other applications', Liège, Belgium, 6–9 October 1986, CRM, 945–954.
4. T. YAMAGATA, H. HARADA, S. NAKAZAWA, M. YAMAZAKI, and Y. G. NAKAGAWA: in Proc. Conf. 'Superalloys 1984', Warrendale, PA, 7–11 October, 1984, The Metallurgical Society of AIME, 157–166.
5. K. A. STROUD: 'Further engineering mathematics', 73; 1986, London, Macmillan Education.
6. H. HARADA: Special Report, National Research Institute for Metals, Tokyo, Japan, 1985.
7. E. NEMBACH and G. NEIIE: *Prog. Mater. Sci.*, 1986, **29**, 177–319.
8. P. R. SAHM and M. O. SPEIDEL (eds.): 'High temperature materials in gas turbines', 115–147; 1974, New York, Elsevier.
9. 'High temperature, high strength nickel base alloys', Special Report, International Nickel Japan Ltd, Tokyo, Japan.
10. S. J. ROSENBERG: 'Nickel and its alloys', Monograph 106, US Department of Commerce, National Bureau of Standards, 1968, 38.
11. S. ATAMERT and H. K. D. H. BHADESHIA: in Proc. Conf. 'Heat treatment 87', The Institute of Metals, May 1987, 39–43.
12. M. RAGHAVAN, R. R. MUELLER, G. A. VAUGHN, and S. FLOREEN: *Metall. Trans.*, 1984, **15A**, 783–792.
13. M. RAGHAVAN, B. J. BERKOWITZ, and J. C. SCANLON: *Metall. Trans.*, 1986, **13A**, 979–984.
14. M. J. CIESLAK, T. J. HEADLEY, and A. D. ROMIG: *Metall. Trans.*, 1986, **17A**, 2035–2047.